Title

Cell expansion-division under resource sharing: a novel framework for modeling fruit growth dynamics

Authors

Leonardo Miele [1,2,*], Lionel Roques [3], Dario Constantinescu [2], Michel Génard [2], Nadia Bertin [2]

[1] Laboratoire Charles Coulomb (L2C), Université de Montpellier, CNRS, Montpellier, France

[2] INRAE, UR1115 Plantes et Systèmes de culture Horticoles (PSH), Site Agroparc, 84914 Avignon, France.

[3] INRAE, UR546 Biostatistique et Processus Spatiaux (BioSp), Site Agroparc, 84914 Avignon, France.

[*] Corresponding author: `mieleo91@gmail.com`

Abstract

Understanding the complex dynamics of fruit growth is crucial for optimizing agricultural practices and improving food production. Observational difficulties pose a challenge to the development of models capable of providing a description of the cellular processes involved, while reproducing the macroscopic observables of interest. Here we present a mechanistic framework for modeling the growth of fleshy fruits. The framework integrates single cell expansion and division processes with organ-wide resource sharing processes. Using empirical data on tomato fruit growth under different irrigation and fruit charge regimes, our model accurately reproduces the temporal patterns of total cell number and fruit mass, and predicts cell mass distributions at harvest. The framework allows for the separation of the effects of

genotypic and environmental factors on the parameters related to the biological processes. This sheds light on the possible relationship between genetic traits, growth conditions and fruit quality traits. In addition, our framework provides insights into the possible mechanisms of nutrient optimization and offers valuable implications for improving agricultural practices. Our study provides a unified approach to fruit growth that can be applied beyond tomato to other multicellular proliferating populations characterized by resource sharing.

Keywords

division-expansion | source-sink | mathematical modeling | fruit growth | Population-Balance Equation | tomato

Introduction

Harvested fruits represent the culmination of complex processes involving cellular, multicellular and human components. Cell expansion is considered to be the most significant factor influencing the final size of the fruit [1, 2], which is a crucial determinant for growers. Cell division is necessary to produce differentiated tissue, it determines the final total number of cells and therefore affects many properties such as texture, firmness and nutrient content [3, 4]. Both expansion and division processes are regulated by plant and environmental cues [5]. These processes require carbon and nitrogen to function, which are provided through water transport and shared among cells.

In light of the mounting global demand for food and the imperative to minimize environmental impact [6], significant research efforts are being directed to understanding the interactions between agricultural, genetic and environmental factors and their influence on fruit quality, with the aim of enhancing yield indicators and reducing water consumption.

Tomatoes (*Solanum lycopersicum*) are a model species for fleshy fruit biology, due to their short life cycle, their great genotypic [7] and phenotypic [8] diversity, and their economic and nutrient importance. Consequently, they represent a privileged system for the study of the effects of molecular mechanisms and agricultural practices on fruit growth [9, 10].

Integrating experimental and theoretical knowledge is hindered by inherent challenges in studying many fruit systems. Indeed, observing the behavior of fleshy fruit cells *in vitro* is inherently problematic as it involves disrupting the 3D structure, thereby interrupting the processes of interest. Furthermore, fruit growth spans several weeks and goes through diverse phases, making comprehensive *in vivo* observation with cellular resolution throughout the entire process very challenging to obtain [11]. Instead, macroscopic observations such as total cell number and mass are more accessible experimentally. Typically, when measured throughout development, such data display sigmoid patterns, as documented for fruits [12, 13, 14] and leaves [15, 16, 17]. This behavior, markedly different from that of a clonal population exponentially colonizing a Petri dish, cannot be explained by the simple sum of single-cell behaviors [18], and requires the invocation of collective or plant-cell regulation arguments [19].

In coping with the aforementioned experimental complications and information lacks, researchers have developed statistical and dynamical models. Statistical models have successfully captured the characteristic saturating patterns observed in plant tissues through the use of logistic-like, parametric curves [20, 21, 12, 22]. While helpful for highlighting the general properties of growth patterns, this approach cannot elucidate the role of the underlying biological mechanisms and their impact on growth dynamics. In contrast, dynamical models aim at incorporating biological processes by means of a mechanistic description of the cell behaviors [23, 24, 25, 26].

Dynamical models of fruit growth often posit a temporal separation between periods of cell division and expansion. This assumption allows for the capture of temporal patterns of

either total cell number [27] or total mass [28, 29, 30]. Similarly, models of resource sharing, which are employed to explain patterns of mass growth at various levels of plant organization [31, 32, 33], are generally developed under the simplification of no cell division [34, 35]. However, such view is very simplistic, as expansion and division processes overlap during the initial stages of fruit development [36, 37, 38]. Furthermore, the above approaches hinder our comprehension of how expansion, division and resource sharing processes collectively influence cell mass distributions.

In light of the complex relations between cellular, tissue and organ scales and the impact of the cellular scale on the regulation of many processes that determine final size and major quality traits, there is a pressing need to develop models integrating expansion and division timescales. Few attempts have been made in this direction. In [39], division occurs according to internal clocks mimicking cell cycles, independently from expansion and resource sharing. While capturing observed patters of tomato fruit cell number and mass, most of the focus however is oriented towards elucidating the role played by genetic material content. Moreover, no attempt is made in fitting the observed mass distributions. In [25], cells either expand or divide, depending on predefined functions of cell age. While incorporating resource-sharing concepts, the model does not provide information on cell size distributions nor how they relate to the processes.

In this study, we propose a unifying framework aimed at bridging the gap between the aforementioned approaches. We develop a general, mechanistic model describing the division-expansion dynamics within a population of cells sharing a common resource. Conceptually, our framework integrates two well-established theories developed independently. Firstly, we draw upon the size-dependent description of the expansion and division processes [40], a framework commonly applied to bacteria [41], plankton [42] and microalgae [43]. Secondly, we incorporate the source-sink formalism to characterize resource flow and sharing between cells, as extensively employed in plant physiology [31, 44, 45].

We apply this framework to both existing and novel empirical data, including experiments investigating the effects of genotype and of agricultural practices on tomato fruit growth. We successfully reproduce the typical temporal patterns observed in both total cell number and fruit mass. Furthermore, our model provides good agreement between predicted and observed cell mass distributions at harvest. We disentangle the different effects that genotype, fruit charge and irrigation regime exert on the model parameters, providing valuable insights into their influences.

Finally, we discuss the implication of our findings for fruit yield and quality optimization and highlight the potential for extending our framework to investigate important size-related metabolic processes. By relying on minimal and general assumptions, our work hold promises for application to other multicellular systems characterized by expansion, division and resource sharing.

Model

In a schematic representation, the fruit is a population of cells connected to the plant through resource pathways including xylem and phloem tissues [45]. Acting as a source of resources, the plant supplies nutrients through the pathway to the fruit, driven by the sink force exerted by fruit cells. Fruit cells uptake these resources and convert part of it into new mass, while part is consumed to cover metabolic costs of maintenance. Cell exist in two states: Proliferating (P) and quiescent (Q). P cells both expand and divide, whereas Q cell can only expand. Furthermore P cells can also differentiate and turn into Q, but the reverse transition does not occur. Evidence shows that once a plant cell loses its proliferation activity, it becomes irreversible [9, 46].

The central hypothesis of our model are the following: i) the processes of expansion and division depend on cell mass [47], and on the concentration of extracellular resources available

from the common source [45]; *ii*) the resource available to fruit cells is the result of a offer-demand flux balance between the source-plant and the fruit-sink [35]; *iii*) differentiation occurs at constant rate.

The population's state at time t is entirely determined by the densities (*i.e.* numbers per mass unit) $n_P(t,x)$ and $n_Q(t,x)$ of P and of Q cells, respectively, with mass x, which serves as a proxy for cell size. From these state variables, any macroscopic quantity of interest, such as the population total cell number $N(t)$ or mass $M(t)$, can be calculated through integration over the mass space, as summarized in Table 1. The aforementioned hypotheses are translated into mathematical laws describing the mechanistic process occurring at the single-cell level: a growth function $\phi(x)$, describing the rate at which a cell of mass x increases its mass; a division function $\gamma(x)$, describing the rate at which a parent cell of mass x divides into two offspring cells; a functional term $\mathbf{\Omega}\left[n(t,\cdot)\right]$, which depends on the state of the entire population (here the $n(t,\cdot)$ notation stresses the temporal dependence), describing how the common resource is shared between cells; a constant ρ describing the rate at which cells differentiate from P to Q.

By invoking standard conservation laws on the above processes [40], we derive equations governing the temporal dynamics of the population:

$$\frac{\partial n_P(t,x)}{\partial t} = \mathbf{\Omega}\left[n(t,\cdot)\right]\left\{-\frac{\partial}{\partial x}\left[\phi(x)\, n_P(t,x)\right] + 4\gamma(2x)n_P(t,2x) - \gamma(x)n_P(t,x)\right\} - \rho n_P(t,x) \tag{1a}$$

$$\frac{\partial n_Q(t,x)}{\partial t} = \mathbf{\Omega}\left[n(t,\cdot)\right]\left\{-\frac{\partial}{\partial x}\left[\phi(x)\, n_Q(t,x)\right]\right\} + \rho n_P(t,x). \tag{1b}$$

In Eq. (1a), the first term in the curly brackets represents the expansion process of P cells, equivalent to a transport in the mass domain with velocity ϕ. The second term represents the gain in number due to parent cells of mass $2x$ dividing into two offspring cells of equal

mass x. The third term represents the loss due to parent cells of mass x dividing. Finally, the last term represents the loss of P cells due to differentiation. Similarly, in Eq. (1b), the first term represents expansion of Q cells, while the second term represents the gain due to P cells turning Q.

The functional term $\mathbf{\Omega}$ represents resource sharing within cells, which affects all mass-dependent processes (gathered inside the curly brackets). Crucially, such term is not externally introduced; rather, its emergence is due to a source-sink balance between the plant and the fruit cells (details in the Materials and Methods). Consequently, expansion and division events ultimately depend not only on single-cell state x, but also on the overall state of the population.

This formulation falls into the class of Population Balance Equations (PBEs), and describes in general terms the expansion-division dynamics of a population of cells sharing a common resource. The exact dynamics depends on the form of the growth and division functions, whose specification can be driven by the knowledge of the biology of the system of interest. Due to its non-local, integro-differential nature, the system Eq. 1 cannot be solved analytical [48], but it has been integrated numerically upon adaptation of typical schemes [49, 50]. The numerical scheme proposed relies on choices and approximations required to overcome the complexities characterizing the systems' dynamics. The scheme is detailed in the Materials and Methods. The Python scripts can be found here.

Parametrization

According to standard considerations on cell physiology, cells grow via uptake of resource through the membrane. The uptake rate is considered proportional to the number of transporters present on the cell membrane, which in first approximation increases linearly with cell surface, leading to a 2/3-power of cell mass. Observations on meristem cells confirm this

argument [51]. Therefore, the mass-dependent growth function is chosen as:

$$\phi(x) = r\, x^{\frac{2}{3}}, \tag{2}$$

where r $\left[\mu g^{1/3}\text{day}^{-1}\right]$ is an effective growth coefficient (per time unit). The larger the value of r, the faster the cell converts resource into new mass. The effective growth coefficient results from the compound contribution of several mechanistic parameters related to respiration cost, uptake speed and mass conversion, as detailed in the Materials and Methods.

Calculations of the source-sink balance of fluxes show that resource-sharing functional depends on the overall uptake demand, and is therefore determined by the function chosen for cell uptake Eq. (2). After some simplifications introduced to reduce parameters number, we obtain the following form (details in Material and Methods):

$$\Omega[n(t,\cdot)] = 1 - \frac{\int n(t,x)\, x^{\frac{2}{3}} dx}{K}, \tag{3}$$

where the parameter K $\left[\mu g^{5/3}\right]$ is an effective carrying capacity for the total resource demand that the fruit is able to produce. We refer to it as a carrying capacity because it regulates the mass the fruit will eventually reach: fruits with larger K will be larger at harvest. Similarly to parameter r, we call it effective because it depends compoundly on total resource concentration, phloem conductance and single-cell uptake rate (details in Material and Methods). Since total demand (the integral in Eq. (3)) can only increase as the population grows, the functional Ω is a decreasing quantity over time and is therefore responsible for the slowing down of the expansion and division processes.

Contrary to prokaryotic cells, the absence of extensive real time data on fruit cells does not allow us to infer the rate of division as function of mass. Instead of introducing further

arbitrary, we have chosen the parametric Hill function proposed in [41]:

$$\gamma(x) = 223.2\,\frac{x^{12}}{h^{12} + x^{12}}, \tag{4}$$

where the parameter h $[\mu g]$ determines the mass at which division rate reaches half-saturation. The larger the value of h, the larger will be the mass at which cells divide on average. The prefactor 223.2 $[\text{day}^{-1}]$ represents a maximal baseline division rate, and it has been set consistently with [41].

To summarize, we obtain a parametrization that is ultimately specified by four effective parameters of biological significance, one for each process (summarized in Table 2): r for expansion, K for resource sharing, h for division, and ρ for differentiation. Standard Bayesian parameter estimation is performed on the available datasets (details in Materials and Methods).

The model is initialized with a genotype-dependent initial number of cells (all in the P state) in accordance with previous estimations [39]. The initial mass distribution is taken as peaked on small values, in accordance with observations on tomato ovary cells [36, 1].

Experimental datasets

The model is fitted on datasets from three different experiments (one already published and two original ones), conducted to investigate genotypic and environmental effects on tomato (*Solanum lycopersicum*) fruit growth. In Experiment 1, tomato plants of a large-fruit - *Levovil* - and a cherry - *Cervil* - genotype are grown with either strong or weak fruit charge: plants cultivated with a high fruit charge are maintained with a low ratio between leaves and fruits (20 per truss for *Cervil* and 6 per truss for *Levovil*), whereas those with a low fruit charge exhibit a high ratio (5 per truss for *Cervil* and 2 per truss for *Levovil*). The four datasets consist of number of cells and fruit mass measured at different development stages,

as well as the mass cell distribution measured on fruits at harvest. In Experiment 2, cherry tomato plants (*Solanum lycopersicum*), line West Virginia 106 (WV106) were grown in a glasshouse either under control or water deficit irrigation. In the control regime water was supplied in order to meet the plant requirements based on the actual evapotranspiration. In the deficit irrigation, the water supply was reduced by half compared to the control. The two datasets consist of number of cells and fruit mass measured at different development stages, but no mass cell distribution is provided. In Experiment 3, *Levovil* plants were grown in a glasshouse either under control irrigation (as above) or deficit irrigation induced by a 40% reduction of water supply. The two datasets consist of fruit mass measured at different stages as for the other experiments. However, here the number of cell is provided only at harvest (together with mass distribution). Details on Experiment 1 can be found in [39], while for Experiments 2 and 3 we remand the Materials and Methods section.

Results

Temporal patterns

Fig. 1 illustrates the temporal evolution of total cell number and fresh mass throughout fruit growth. The solid curves correspond to the model's predictions, obtained using the best-fit parameters. The scatter symbols correspond to experimental data. Time is measured in days after anthesis (DAA).

The model is able to reproduce simultaneously the kinetics of cell number and fruit mass observed in all experiments. This includes the three-phase behavior typical of fruit cells. Firstly, a phase driven by exponentially-like number and mass increase. In this phase, the resource sharing contribution Ω is far from carrying capacity, so that the number kinetics is dominated by division while cells expand at close to maximal rate. The duration of this

phase ends at around DAA = 10 for cherry tomatoes, and at around DAA = 20 for large ones, in line with experimental data. As fruit mass increases, cell resource uptake decreases due to a reduction in the resource-sharing contribution, thereby initiating a second phase of linear growth. This phase is slightly asynchronous between numbers and masses due to the concurrent differentiation of P cells into Q cells, which contributes to the mitigation of division. The feedback between single-cell uptake and total fruit mass resolves into a final, third phase. In this phase, the total cell number stops increasing because the cell division rate drops below the differentiation rate, thus emptying the compartment of P cells. Once all cells have turned quiescent, the total number reaches the plateau determining the final number of cells at harvest. In contrast, fruit mass exhibits a sub-linear increase, due to Ω approaching the carrying capacity.

Cell mass distributions

Fig. 2 shows this dynamics for the *Cervil*-weak case, obtained from the posterior mode associated with the corresponding dataset. The diagram vividly illustrates a non-trivial behavior, characterized by non-monotonic evolution of the function $t \mapsto n(t, x)$, particularly noticeable at lower mass ranges. At first, expansion drives cells towards values of x close to half-saturation h. Cells undergo extensive rounds of division around mass h, continuously splitting into smaller cells which are promptly pushed by expansion towards values close to h. This process produces a cascade of division events which coincides with the first exponentially-like kinetic behaviors. Concurrently, differentiation generates a sub-population of cells that escape division and start increasing their mass above values of h, contributing to cell heterogeneity. When cell division ceases due to extinction of the division rate, mass heterogeneity keeps increasing, driven by the differences in resource uptake provided by $\phi(x)$.

In Fig. 3, we compare the final distributions predicted by the model (obtained with best-fit parameters) with the available experimental data measured at harvest. The model

reproduces the observed features, including non-trivial long tails and peaks in small mass values. It is important to note that these data were used solely for validation purposes and not for parameter estimation. For Experiment 2, for which such data are not available, the model provides the expected distribution.

Disentangling genotypic and environmental effects

In Fig. 4, we present the posterior obtained from Bayesian estimation and highlight the best-fit parameter values for each dataset, with errorbars indicating the corresponding standard deviations. Particularly, we focus on differences within experiments, as we cannot exclude that between-experiments might be due to different environmental conditions (*e.g.* greenhouse temperature). Results are summarized in Table 2, displaying increases ($\nearrow$) or decreases ($\searrow$) of the values of the best-fit parameters with respect to agricultural practices.

Growth conditions show minimal impact on the effective growth coefficient r across experiments (panel A), with the exception of Experiment 3. Differentiation rate ρ is significantly influenced by both fruit charge and irrigation conditions (panel B). The carrying capacity, denoted by K, is affected by the genotype and growth conditions. Large-fruit genotypes tend to exhibit higher values (as expected), while water-deficit and high fruit charge tend to reduce it (panel C). Finally, fruit charge affects the half-saturation mass h in large-fruit genotypes but not in cherry ones.

Discussion and Conclusions

The importance of size in plant single-cell's development is unequivocal [52]. The regulation of plant organ and cell size depends on interrelated factors that are not yet fully understood, mainly due to observational limitations. Modern microscopy and cell-tracking techniques are now commonly used to study the behavior of prokaryotic cells [53, 41, 54], and allow to

opt in or out the different possible hypotheses [55, 56], a way that is hardly applicable to fruit systems. Most of the *in vivo* knowledge to date is based on the model plant *Arabidopsis thaliana*. [57], whose solid fruit is very different from the fleshy fruits that make up the human diet worldwide. Here, we have developed a mechanistic framework of fruit growth that focuses on the three indispensable processes: cell expansion, cell division and resource sharing.

When applied to empirical data on tomato fruit growth, our model reproduces well the typical sigmoid temporal patterns observed in total cell number and fruit mass, from anthesis to harvest, and under different irrigation and fruit charge regimes (Fig. 1). In addition, our model provides insights into the hidden dynamics of cell mass distribution during growth (Fig. 2). It also accurately estimates the cell mass distribution at harvest, capturing both the long tail and the high peak for smaller masses (Fig. 3).

Crucially, our fitting procedure relies on macroscopic data (total cell number and mass) and is independent of cell mass distribution data. This offers several advantages. Firstly, it highlights the robustness of our approach and provides an autonomous validation of the chosen cell growth Eq. (2) and division Eq. (4) laws. Indeed, preliminary explorations of the model's behaviors indicated that a linear expansion law would yield accurate kinetics for cell number and mass but would generate inaccurate distributions (not shown). Secondly, determining cell mass distributions in plant tissues involves sample disruption, rendering the process expensive and delicate, and variations in techniques may also introduce biases [58].

By bypassing the necessity for cell mass distribution data in the fitting process, our model presents a cost-effective and non-invasive alternative to both make predictions on incomplete datasets (as we did for Experiment 2), and to perform *in silico* experiments (mimicking genetic or environmental modifications). Total cell number estimations from fruit tissue extraction can be time-consuming and subject to measurement errors, leading to few point of measurement and high uncertainties in data [58]. Encouragingly, Experiment

3 shows that measurements at harvest can suffice for good fits. On the other hand, future applications of the model would benefit from precise estimations of cell numbers at very early stages. While evidence suggests environmental effects may manifest as early as the ovarian development period, their impact on pre-anthesis cell number appears limited [59]. Thus, such measurements could be leveraged to establish genotype-dependent initial conditions for the model, regardless of the growth conditions that will subsequently be employed during the experiment.

In order to reproduce the sigmoid patterns typical of plant tissue, previous work relied on the introduction of temporal brakes, which mimicked metabolic regulation [39, 25]. Although we acknowledge the significance of metabolic regulation in coordinating the mechanisms that underlie plant cells development [60, 61, 46], we argue that its implementation requires extensive parametrization than ours, which may lead to overfitting issues when applied to data-poor systems, such as fruit cells [62]. In contrast, our formulation proposes the shift to a resource-based framework. The balance between a resource supply and an increasing demand leads to the emergence of a contribution that depends on the whole population state (here represented by Ω). Ultimately, this contribution is responsible for the deceleration of the size-dependent processes (here expansion and division).

We argue that the shift from a time-based to a resource-based regulation has several advantages. First, it could allow to explore Gene x Environment x Phenotype (GxExP) effects onto resource allocation and yield production [46], *e.g.* by simulating irrigation practices. Here, we have prioritized simplicity and considered a constant resource supply during the dynamics. However, extensions to temporal variations can be implemented straightforwardly. For example, a common field experiment involves combining a full irrigation regime for the first weeks after anthesis with a subsequent water stress regime. In our dynamical formalism, this would result in temporally variable carrying capacity, $K(t)$, and growth coefficient, $r(t)$, which would modulate variations in the growth and division processes over time. These

variations would then have consequences on the fruit weight and composition, which could then be compared with experiments.

Second, our minimal formulation requires the estimation of only 4 parameters, which relate to fundamental mechanistic processes. The introduction of further mechanisms could lead to non-identifiability issues, potentially masking their effects on the dynamics, unless supported by experimental evidence. For instance, Eqs. (1)-(2)-(4) herein used are expected to be applicable also to other single sigmoidal growth patterns, such as those observed in apples [63], cucumber [64], olives [65], eggplant, pepper and kiwifruit [66]. However, such simple choices will not be able to capture the double sigmoidal growth patterns characteristic of other fruits, such as peaches and strawberries [63, 67]. Indeed, recent evidence from transcriptome analysis suggests that these patterns may arise from distinct expansion behaviors due to regulatory networks activated at different developmental stages [68], which would translate into two distinct (rather than one) single-cell expansion laws. An alternative, plausible explanation for the emergence of double-sigmoids could be provided by a more complex differentiation process than the one herein considered, which would result in the addition of a second quiescent class. If supported by biological information on the parametrization of the above processes, our mechanistic framework could be used to test and compare the two possibilities.

Our mechanistic formulation of the processes provides insights into the environmental impact on these mechanisms (Fig. 3), summarized in Table 2. Increased fruit charge leads to smaller fruits, with fewer but larger cells on average. This results in a reduced effective carrying capacity K and differentiation rate ρ, and in an increased half-saturation division mass h. The decrease in K can likely be attributed to phloem conductance corrections occurring at the fruit organizational level (see Eq. (9b)), consistent with previous findings [31]. Interestingly, inspection of Eqs. (9a) and (9b) suggests that potential genetic variations on single-cell resource uptake could be inferred by examining the inverse relationship between

K and r.

Some studies have proposed the existence of a compromise between resource uptake and fruit size, which would result in a trade-off between the values of r and of K. Our results do not permit a definitive conclusion to be drawn, as the estimated values of r are found to be similar for both the large-fruit genotypes (*Levovil*) and the cherry genotypes (*Cervil* and *WV106*). Nevertheless, our model could contribute to the validation of this compromise, provided that further data on experiments where different genotypes are grown under the same environmental conditions becomes available.

The h parameter is related to division: with high h cells must be bigger to have the half probability of division. A higher h value in conditions of lack of resource (high fruit charge or water deficit) suggests that in lack of resources cells tend to slower division. This could be a strategy of resource uptake, since cells exploit the resources to expand, rather than dividing. At the end of the process, indeed, the global number of cells is slower in lack of resources. Coherently, a lower value for the quiescence rate ρ in water deficit and high charge suggests that in lack of resources, cells tend to undergo more division events before entering into quiescence. While not clearly interpretable, this simulated phenomenon is interesting for studying the endoreduplication in further development of the model and deserves interest, since in many fruit species cells start an expansion process linked to ploidy increase (endoreduplication) when entering quiescence [69, 70].

Our model allows for the reconstruction of the unobserved temporal dynamics of mass distribution. The nonlinear trajectory shows that the interplay between cellular expansion, division, and nonlocal interactions gives rise to non-trivial dynamical patterns, which defy simple statistical models and reaffirm the advantage of dynamical ones. The emerging dynamics (Fig. 2) is consistent with temporal patterns observed experimentally in other fruit systems [63], and offers a mechanistic framework to support experimental research in food quality. For instance, cell mass distributions can be used to infer the micro-mechanical prop-

erties of cell walls [71], which in turn affect several fruit quality traits, such as: texture [72], juiciness [73] and sugar content.

The framework could be integrated with a dynamic module for the production of cell organelles, such as plastids. Indeed, evidence show that the division rate of chloroplasts is influenced by regulatory mechanisms related to both cell division and size [74, 75]. The abundance of chloroplast is also considered to be a limiting factor for carotenoid formation, which are fundamental compounds for fruit organoleptic quality [3]. Incorporating chloroplasts dynamics into our cell mass distribution evolution could therefore provide a tool to investigate chloroplast formations and its relationship with agricultural practices.

We conclude with a remark on the general significance of our study. We have obtained a novel class of PBEs, which features feedback between population and single-cell levels. This dynamics differs from that of previous PBE formulations, which considered extracellular resource dynamics [76], employed to model *in vitro* [77] or bioreactor [78, 43, 79] environments, where cell populations cease to proliferate due to resource depletion. We consider this mechanism to be inherent to all multicellular systems where cells draw resources from a shared pool to fuel expansion and division. Therefore, we propose our formalism as a foundation for the analysis of the population dynamics of such systems. Our derivation stems from fruit growth, but it is expected to be applicable to other plant tissues, such as leaves and seeds, as well as biofilm and cancer tissues, which exhibit similar behaviors [80, 81]. The introduction of our new class of PBEs expands the range of dynamics related to cell expansion and division, paving the way for further applications and analysis.

Materials and Methods

Experiment 2

In experiment 2, cherry tomato plants (*Solanum lycopersicum*), line *West Virginia 106* (*WV106*) were grown at a plant density of $2.2\,\text{plants}\,m^{-2}$ in a glasshouse in Avignon (south of France) from April to August. The day-night temperature set-point was $22°C - 16°C$. Plants were planted in $7\,l$ pots filled with potting soil (Klasmann, Substrat SP 15%) and an irrigation treatment was applied as soon as the first flowering truss appeared: 4 blocks of 5 plants were placed under "well-watered" irrigation conditions and 4 blocks of 5 plants were placed under "water-deficit" conditions, spread over 6 rows of 15 plants surrounded by border plants. The "well-watered" condition met the plant's water requirements defined on the basis of the ETP measured in the greenhouse. For the water deficit, irrigation volumes were reduced by half compared with the control, without changing the frequency. The two treatments corresponded to a substrate water content of around 1.5 and 0.8 $gH20g^{-1}$ dry soil for the control and deficit respectively. Nutrients were provided by fertigation ($EC \approx 2.0$ to $3\,mS\,cm^{-1}$, $pH \approx 6$) and no salinity stress occurred. Flowering trusses were pruned to a maximum of $8 - 10$ fruits, and flowers were hand-pollinated 3 times a week. Anthesis was recorded on each truss and fruits were harvested according to the number of Days After Anthesis (DAA). Fruits were harvested between 2 DAA and maturity on 5 different trusses avoiding distal positions in the inflorescence. Fresh and dry fruit weights were measured as soon after sampling and after drying in a ventilated oven at $65°C$. The number of pericarp cells was measured after enzymatic digestion of the walls and release of suspended cells as described in [27]. Cells were counted in aliquots of a cell suspension under an optical microscope using Fuchs–Rosenthal chambers and Bürker chambers for the large and small fruit, respectively. Six to eight aliquots per fruit were observed and the cell number for the whole

pericarp was calculated according to the dilution and observation volumes. In addition, cell-size distributions (smallest and largest radii and 2D-surface) in the cell suspension aliquots were measured on ripe fruit using the ImageJ software (https://imagej.nih.gov/ij/). Five samples of $\sim$ 20–25 cells per fruit pericarp were measured randomly for different fruits, so that around $300 - 500$ cells were counted for each treatment.

Experiment 3

Levovil plants (*Solanum lycopersicum*) were grown at a plant density of $2.4\,\text{plants}\,m^{-2}$ in a glasshouse in Bellegarde (South of France) from 1st February to June. The day-night temperature regime was monitored to $20 - 16°C$. From flowering of the third truss, two water regimes were applied: well-watered plants were irrigated according to current practices (25% drainage); water-deficit plants were irrigated with a 40% decrease of water supply. Nutrients were provided by fertigation ($EC \approx 2.0$ to $3\,mS\,cm^{-1}$, $pH \approx 6$) and no salinity stress occurred. Flowering trusses were pruned to a maximum of 6 fruits, and flowers were pollinated by bumblebees. Fruits were harvested between 5 DAA and maturity (red-ripe stage) on 5 different trusses avoiding distal positions in the inflorescence. Fresh and dry fruit weights were measured as soon after sampling and after drying in a ventilated oven at $65°C$. At the red ripe stage, pericarp cell number and cell size distributions were measured on 6 fruits of each treatment, as described for Experiment 2.

Microscopic processes - Cell expansion

In a minimal mechanistic description, a cell grows through uptake of the resource allocated to it. Part of such resource is converted into novel mass, while part of it is consumed in order to maintain the metabolic machinery. Cell growth rate is proportional to a mass-dependent uptake function $u(x)$ [26], and to the concentration R_f of resource available to the fruit

(generalization to non-linear cases is straightforward [31], and is herein avoided in order to reduce the number of parameters). Therefore, a cell with mass x grows according to the following ordinary differential equation:

$$\frac{dx}{dt} = c\, r_0\, [R_f - s]\, \tilde{\phi}(x), \tag{5}$$

where $c\, \left[\mu g^{\,[u(x)]+1}\right]$ is a resource-to-biomass conversion coefficient, $R_f\ [\mu g\, V]$ is the resource concentration available to the fruit, $s\ [\mu g\, V]$ is the metabolic discount, and $u(x)\ [u(x)]$ is the uptake rate per resource concentration function. Metabolic discount includes resource consumption by respiration, whose rate in tomatoes is proportional to mass growth rates [82]. The resource concentration R_f exploited by cells is obtained by invoking source-sink flux balance [31, 35, 45]. The resource flux $\mathcal{F}\left[\mu g\, \mathrm{day}^{-1}\right]$ from the source to the sink is:

$$\mathcal{F} = f_0\, R\, \left(R - R_f\right), \tag{6}$$

where $f_0\left[\mu g^{\,-1} V^2 \mathrm{day}^{-1}\right]$ is the transfer pathway's conductance, and $R\left[\mu g V^{-1}\right]$ is the total resource concentration at the source. The unloading $\mathcal{U}\left[\mu g\, \mathrm{day}^{-1}\right]$ of resource at the sink is provided by the sum of all uptake contributions from all sink cells, that is:

$$\mathcal{U} = r_0 R_f \int N(x,t)\tilde{\phi}(x)dx = r_0 R_f S(t), \tag{7}$$

where $r_0\left[V\, \mu g^{\,[u(x)]+1}\right]$ is the single-cell uptake rate. Assuming an absence of storage capacity within the transfer pathway, we have balance between in and out fluxes. Solving $\mathcal{F} = \mathcal{U}$ for R_f, we get:

$$R_f = \frac{R}{1 + \frac{r_0}{f_0 R} S(t)}. \tag{8}$$

Inserting Eq. (8) into Eq. (5) we get:

$$\frac{dx}{dt} = c\, r_0 \left[\frac{R}{1 + \frac{r_0}{f_0 R} S(t)} - s \right] \tilde{\phi}(x)$$

The three-parameter function $S \mapsto \frac{R}{1+\frac{r_0}{f_0 R} S} - s$ is convex. It equals $R - s$ at $S = 0$ and becomes zero at $S = \frac{f_0 R}{r_0 s}(R - s)$. Thus, its shape mainly depends on the difference $R - s$ rather than solely on the values of R and s. To avoid identifiability issues, we approximate this function with a simpler two-parameter linear function, which intersects the horizontal and vertical axes at the same points as the original function. This approximation leads to:

$$\frac{dx}{dt} = r \left[1 - \frac{S(t)}{K} \right] \tilde{\phi}(x),$$

where

$$r = c\, r_0 (R - s) \quad \left[\mu g^{\,1-[u(x)]}\, \mathrm{day}^{-1} \right] \tag{9a}$$

$$K = \frac{f_0 R}{r_0} \frac{R - s}{s} \quad \left[\mu g^{\,[u(x)]+1} \right] \tag{9b}$$

are the emerging effective compound parameters. Rather than on the five parameters c, r_0, f_0, R and s separately, the model's behavior is therefore best identifiable by the two effective parameters r and K, which can be fitted. Parameter r increases proportionally to resource-mass conversion ε and to source resource concentration R, while it decreases proportionally to metabolic maintenance cost s. Therefore, we refer to it as an effective single-cell growth coefficient. Parameter K increases with phloem conductance f_0 and total resource concentration R, while it decreases with single-cell uptake rate r_0 and metabolic discount s. Since this parameter sets the order of magnitude of the fruit's final size, we refer

to it as an effective carrying capacity. Finally, the single-cell growth law becomes:

$$\frac{dx}{dt} = r\left[1 - \frac{S(t)}{K}\right]\tilde{\phi}(x), \tag{10}$$

where $\Omega[S(t)] = \left[1 - \frac{S(t)}{K}\right]$ and $\phi(x) = r\,\tilde{\phi}(x)$ are the general forms of the, respectively, population and single-cell contributions appearing in Eq. (1).

Microscopic processes - Cell division

The regulation of cell division is driven by both metabolic and environmental cues [46]. In a mechanistic description of cell division, this complexity is generally captured by the introduction of size-dependent behavior. This so-called "sizer" mechanism represents a basic hypothesis of mathematical models [56] and is consistent with observations of root [83] and meristem [51] cells. Accordingly, we define the probability density $\tilde{\gamma}(x)$ of a cell with mass x to divide. The corresponding division rate Γ, appearing in Eq. 1a, is obtained by following standard arguments [48]. The probability of a cell to divide at a mass $\in [x, x + dx]$ is $\tilde{\gamma}(x)dx$. Let Δx be the small mass increase in the small time interval Δt, then the following relation holds:

$$\Gamma\Delta t = \frac{\tilde{\gamma}(x)\Delta x}{1 - \int \tilde{\gamma}(x)dx}. \tag{11}$$

In the limit $\Delta t \to 0$, the single-cell growth law Eq. (10) can be inserted in the above equation and the terms appearing in Eq. (1a) are obtained:

$$\Gamma(x) = \gamma(x)\,\Omega\left[n(t,\cdot)\right], \tag{12}$$

where $\gamma(x) = \frac{\tilde{\gamma}(x)g_1(x)}{1-\int \tilde{\gamma}(x)dx}$ includes all the mass contributions to cell division, while $\Omega\left[n(t,\cdot)\right]$ represents the same population contribution appearing in the mass expansion law.

PDE solver for the main system

In addressing the challenges presented by our model — specifically, initial conditions concentrated near 0 with rapid decay, the need for precision in capturing phenomena close to 0 to accurately describe early cell divisions, ensuring total population conservation in the absence of a reaction term, minimizing numerical diffusion to preserve the distinct effects of growth and division, and the complexity introduced by nonlocal terms that complicate the use of implicit or Crank-Nicolson schemes — we embarked on a comprehensive evaluation of numerical methods. Initial tests with upwind and Lax-Friedrichs schemes revealed excessive numerical diffusion. Although the Lax-Wendroff scheme, enhanced with flux limiters, showed promise in simpler scenarios by significantly reducing numerical diffusion, its application to our problem was hindered. The scheme's reliance on the assumption that time and space derivatives are proportional by a constant factor proved inadequate for our complex model, where such a simplification does not hold, and any attempt to adapt it would require extensive modification.

To overcome these challenges and limitations, we developed a numerical scheme that balances the need for precision, mass conservation, and minimal numerical diffusion. The numerical method uses an explicit Euler scheme in time, a non-uniform grid in space, with grid points more concentrated for small x values. It deals separately with the transport and reaction terms, in two separate steps. To deal with the transport equation, (1) we construct a spatial interpolation of the solution at time t over $(0, L)$; (2) we compute the exact solution at time $t + dt$ based on the solution at time t. To deal with the reaction term, we directly compute the terms in the right-hand side, and use an interpolation to compute the values at positions $2x$. A commented Python version of the solver is available as a Colab notebook here.

Mechanistic-statistical approach

Mechanistic-statistical modeling bridges the gap between the solutions of continuous state models, such as Eq. (1), and empirical data, including noisy discrete data. This approach combines a mechanistic model, a probabilistic observation model that conditionally describes the data based on model outputs, and a statistical inference procedure. Initially applied to physical models and data [84], mechanistic-statistical methods have become increasingly standard in spatial ecology [85]. These methods require a mechanistic model that is not overparameterized, which may explain why their application at the organismal scale, such as in the case of fruits, remains rare.

Observation model The datasets are associated with the solution of Eq. (1) by positing that, for each dataset, the observed number of cells $\hat{N}(t)$ and the observed fruit mass $\hat{M}(t)$ at time t adhere to Normal distributions. These distributions have mean values $N(t)$ and $M(t)$ as provided by Eq. (1) (see Table 1), and standard deviations σ_N and $\sigma_M \times M(t)$, respectively. This assumption is grounded in the observation that the standard deviation of mass measurements tends to be proportional to the mass itself. For each dataset, σ_N and σ_M are calculated directly as the average standard deviation in the data (and standard deviation divided by mass, respectively) across replicate observations (i.e., observations made on the same date).

Statistical inference The parameters r, K, h, and ρ are unknown. We employed a Bayesian method [86] to estimate their posterior distribution.

Computation of the likelihood function. The likelihood $\mathcal{L}$ represents the probability of the observations given the parameters. Using the observation model and assuming independence

of observations conditionally on the underlying biological process, we define:

$$\mathcal{L}_{\mathcal{N}}(r, K, h, \rho) := P(\text{dataset}|r, K, h, \rho) = \prod_{t \in \mathcal{T}_N} \prod_{i \in \#_t} \exp\left(-\frac{|\hat{N}_i(t) - N(t)|^2}{2\sigma_N^2}\right)$$

for the likelihood associated with the number of cells, and:

$$\mathcal{L}_{\mathcal{M}}(r, K, h, \rho) := P(\text{dataset}|r, K, h, \rho) = \prod_{t \in \mathcal{T}_M} \prod_{i \in \#_t} \exp\left(-\frac{|\hat{M}_i(t) - M(t)|^2}{2\sigma_M^2\, M(t)^2}\right)$$

for the likelihood associated with fruit mass. Here, $\mathcal{T}_N$ and $\mathcal{T}_M$ correspond to the measurement times and $\#_t$ to the corresponding number of replicate observations. The overall likelihood $\mathcal{L}(r, K, h, \rho) = \mathcal{L}_{\mathcal{N}} \times \mathcal{L}_{\mathcal{M}}$ depends on the unknown parameters through $N(t)$ and $M(t)$.

Posterior distribution. The posterior distribution reflects the parameter distribution conditional on the observations:

$$P(r, K, h, \rho|\text{dataset}) = \frac{\mathcal{L}(r, K, h, \rho)\, \pi(r, K, h, \rho)}{C}, \tag{13}$$

where $\pi(r, K, h, \rho)$ denotes the prior distribution of the parameters (as detailed below) and C is a normalization constant independent of the parameters.

Prior distribution. We adopted independent, non-informative uniform prior distributions for all parameters, with $r \in (0, 1)$, $K \in (5 \cdot 10^4, 2 \cdot 10^9)$, $h \in (0.05, 1)$, and $\rho \in (0, 1)$.

The numerical computation of the posterior distributions was conducted using a Metropolis-Hastings (MCMC) algorithm with at least $2 \cdot 10^5$ iterations. The Matlab® codes are provided as Supplementary Material. The mean CPU time for solving Eq. (1) was approximately 25

seconds, with the total CPU time for the eight datasets being about 16 months (conducted in parallel over 2 months, on Intel(R) Xeon(R) CPU E5-2637 v3 @ 3.50GH). The corresponding marginal distributions of r, K, h and ρ are shown in Fig.4. We note that these distributions are far from flat, indicating that the datasets do contain information on the parameters.

Acknowledgments

The authors thank Gilles Vercambre for fruitful discussions. This work was funded by an ANR research grant (TomHealth ANR-20-CE21-0010).

Table 1: Notation state variables

Symbol	Description
x	Cell mass ($[\mu g]$)
$n_P(t,x)$	Density of Proliferating cells with mass x at time t
$n_Q(t,x)$	Density of Quiescent cells with mass x at time t
$n(t,x)$	Total cell density $n_P(t,x) + n_Q(t,x)$
$N(t)$	Total Cell Number $\int_0^\infty n(t,x)\,dx$
$M(t)$	Total Fruit Mass $\int_0^\infty x\,n(t,x)\,dx$
$\phi(x)$	Single-cell growth function
$\gamma(x)$	Single-cell division function
$\Omega[n(t,\cdot)]$	Population-level resource-sharing function

Table 2: Environmental effects on best-fit parameters

Symbol	Description	Unit of measure	Water deficit	Fruit charge
r	Effective growth coefficient	$\mu g^{\,1/3}\,\mathrm{day}^{-1}$	$\searrow$	-
K	Effective carrying capacity	$\mu g^{\,5/3}$	$\searrow$	$\searrow$
h	Half-saturation probability division size	μg	$\nearrow$	$\nearrow$
ρ	Differentiation rate	day^{-1}	$\searrow$	$\searrow$

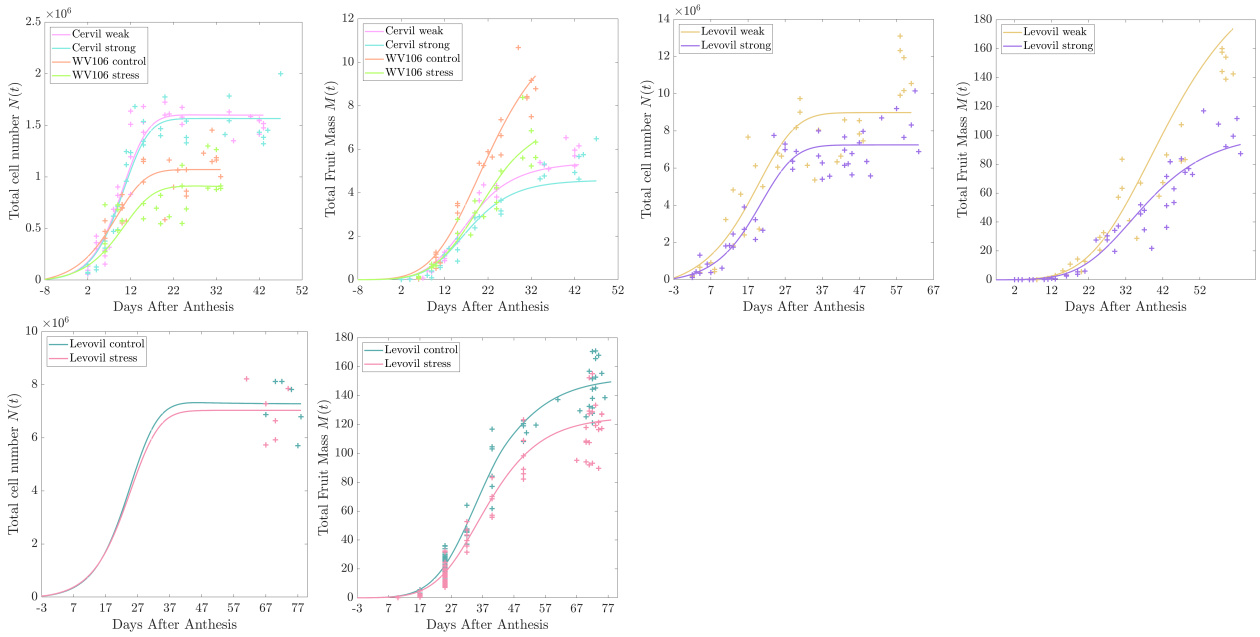

Figure 1: The best fit parametrization reproduces well the temporal patterns of both total cell number and fresh mass, for all the six experimental cases considered. Solid lines represent the model's dynamics, while scatter symbols the datapoints.

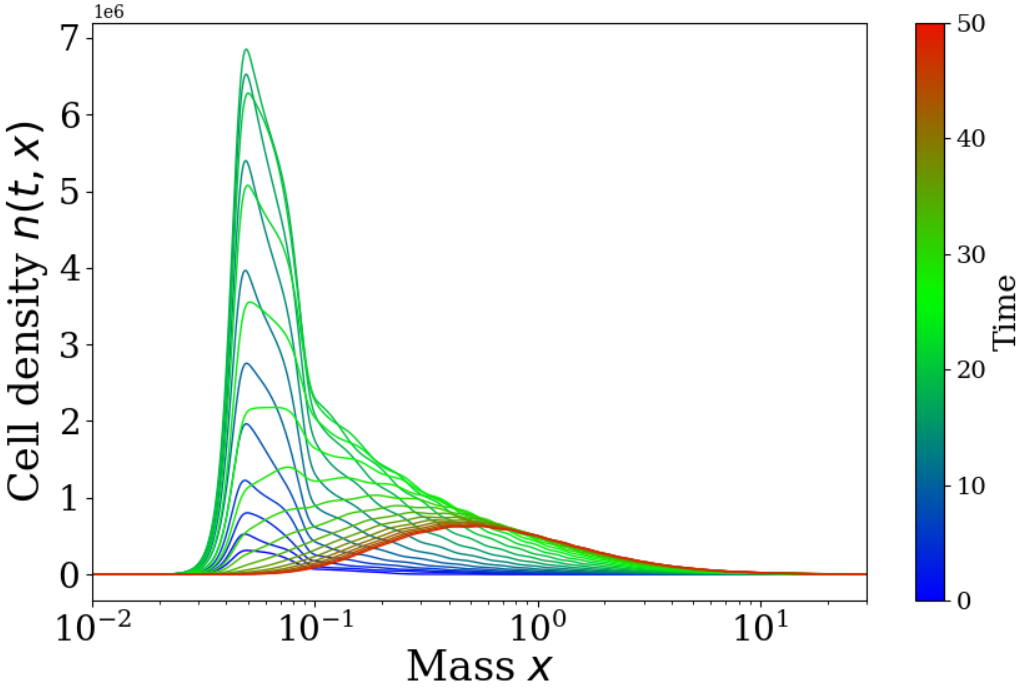

Figure 2: Dynamics of cell mass distribution in the Cervil faible dataset, reconstructed from Eq. (1) using best-fit parameter values.

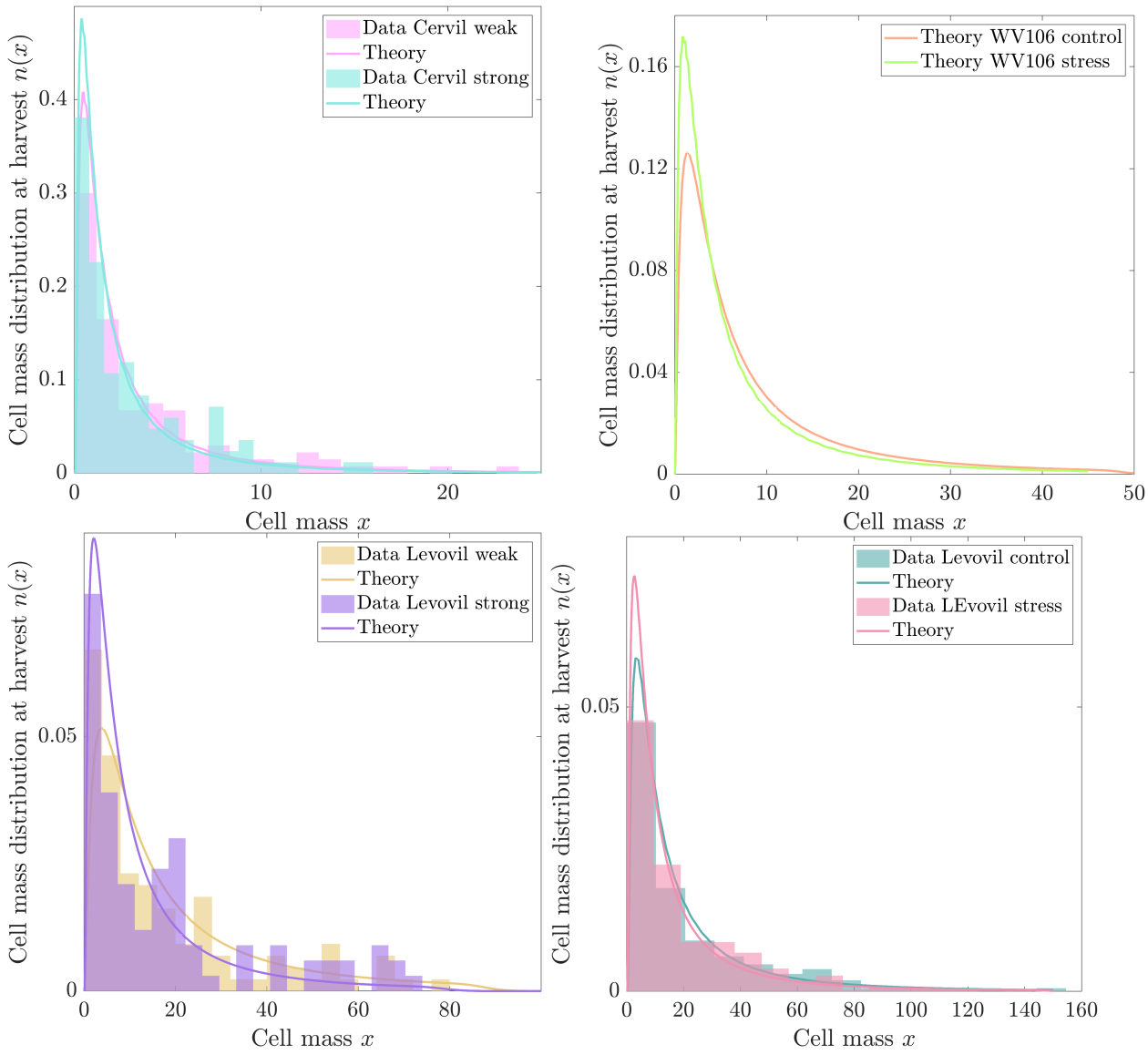

Figure 3: Final cell mass distribution driven by expansion-division under resource-sharing. Solid lines represents the model's prediction, while histograms represent data at harvest.

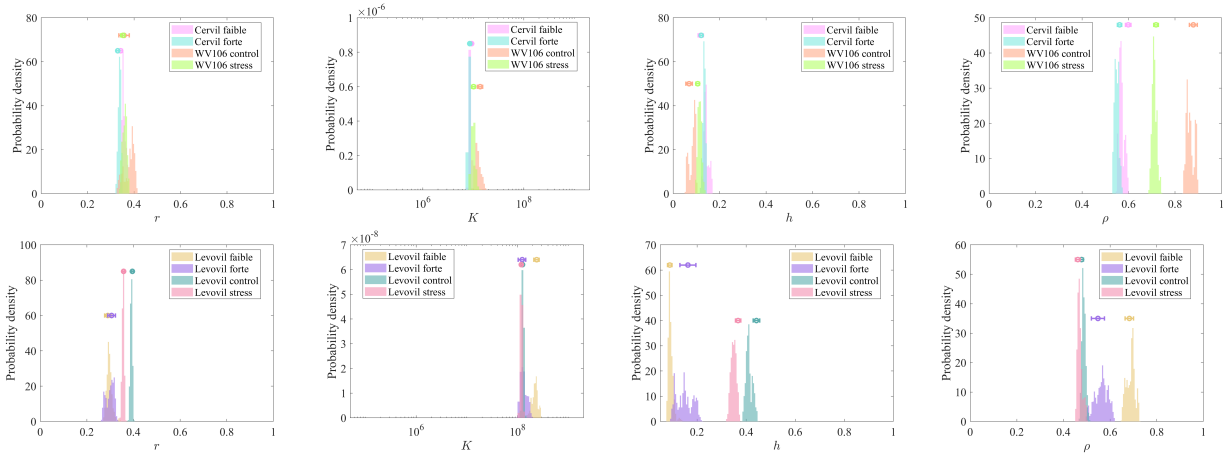

Figure 4: Posterior marginal distributions of the parameters r, K, h, and ρ. Errorbars highlight the corresponding best-fit value $\pm$ standard deviation.

References

[1] Constance Musseau, Daniel Just, Joana Jorly, Frédéric Gévaudant, Annick Moing, Christian Chevalier, Martine Lemaire-Chamley, Christophe Rothan, and Lucie Fernandez. Identification of two new mechanisms that regulate fruit growth by cell expansion in tomato. Frontiers in Plant Science, 8:988, 2017.

[2] Martine Lemaire-Chamley, Johann Petit, Virginie Garcia, Daniel Just, Pierre Baldet, Véronique Germain, Mathilde Fagard, Mariam Mouassite, Catherine Cheniclet, and Christophe Rothan. Changes in transcriptional profiles are associated with early fruit tissue specialization in tomato. Plant Physiology, 139(2):750–769, 2005.

[3] Salvador Torres-Montilla and Manuel Rodriguez-Concepcion. Making extra room for carotenoids in plant cells: New opportunities for biofortification. Progress in Lipid Research, 84:101128, 2021.

[4] Rémy Aurand, Mireille Faurobert, David Page, Jean-François Maingonnat, Béatrice Brunel, Mathilde Causse, and Nadia Bertin. Anatomical and biochemical trait network underlying genetic variations in tomato fruit texture. Euphytica, 187:99–116, 2012.

[5] Enrico Coen and Przemyslaw Prusinkiewicz. Developmental timing in plants. Nature Communications, 15(1):2674, 2024.

[6] David Tilman, Christian Balzer, Jason Hill, and Belinda L Befort. Global food demand and the sustainable intensification of agriculture. Proceedings of the national academy of sciences, 108(50):20260–20264, 2011.

[7] Christophe Rothan, Isidore Diouf, and Mathilde Causse. Trait discovery and editing in tomato. The Plant Journal, 97(1):73–90, 2019.

[8] Véronique Bergougnoux. The history of tomato: from domestication to biopharming. Biotechnology advances, 32(1):170–189, 2014.

[9] Jean-Philippe Mauxion, Christian Chevalier, and Nathalie Gonzalez. Complex cellular and molecular events determining fruit size. Trends in Plant Science, 26(10):1023–1038, 2021.

[10] Nadia Bertin and Michel Génard. Tomato quality as influenced by preharvest factors. Scientia Horticulturae, 233:264–276, 2018.

[11] Leen Van Doorselaer, Pieter Verboven, and Bart Nicolai. Automatic 3d cell segmentation of fruit parenchyma tissue from x-ray micro ct images using deep learning. Plant Methods, 20(1):12, 2024.

[12] Nadia Bertin, Hélène Gautier, and Cédric Roche. Number of cells in tomato fruit depending on fruit position and source-sink balance during plant development. Plant Growth Regulation, 36:105–112, 2002.

[13] Masami Yamaguchi, Takashi Haji, Masanori Miyake, and Hideaki Yaegaki. Varietal differences in cell division and enlargement periods during peach (prunus persica batsch) fruit development. Journal of the Japanese Society for Horticultural Science, 71(2):155–163, 2002.

[14] Joan M Bain and RN Robertson. The physiology of growth in apple fruits i. cell size, cell number, and fruit development. Australian Journal of Biological Sciences, 4(2):75–91, 1951.

[15] Christine Granier, Olivier Turc, and Francois Tardieu. Co-ordination of cell division and tissue expansion in sunflower, tobacco, and pea leaves: dependence or independence of both processes? Journal of Plant Growth Regulation, 19:45–54, 2000.

[16] Alfredo AC Alves and Tim L Setter. Response of cassava leaf area expansion to water deficit: cell proliferation, cell expansion and delayed development. Annals of Botany, 94(4):605–613, 2004.

[17] N Sunderland. Cell division and expansion in the growth of the leaf. Journal of Experimental Botany, 11(1):68–80, 1960.

[18] Christine Granier and Francois Tardieu. Multi-scale phenotyping of leaf expansion in response to environmental changes: the whole is more than the sum of parts. Plant, Cell & Environment, 32(9):1175–1184, 2009.

[19] Valentina Baldazzi, Nadia Bertin, Hidde de Jong, and Michel Génard. Towards multi-scale plant models: integrating cellular networks. Trends in plant science, 17(12):728–736, 2012.

[20] Irene Salinas, Juan José Hueso, and Julián Cuevas. Fruit growth model, thermal requirements and fruit size determinants in papaya cultivars grown under subtropical conditions. Scientia horticulturae, 246:1022–1027, 2019.

[21] MM Avanza, SJ Bramardi, and Silvia Matilde Mazza. Statistical models to describe the fruit growth pattern in sweet orange" valencia late". Spanish Journal of Agricultural Research, 6(4):577–585, 2008.

[22] PW Gandar, AJ Hall, and HN De Silva. Deterministic models for fruit growth. In IV International Symposium on Computer Modelling in Fruit Research and Orchard Management 416, pages 103–112, 1995.

[23] Solomon Workneh Fanta, Metadel K Abera, Wondwosen A Aregawi, Quang Tri Ho, Pieter Verboven, Jan Carmeliet, and Bart M Nicolai. Microscale modeling of coupled water transport and mechanical deformation of fruit tissue during dehydration. Journal of food engineering, 124:86–96, 2014.

[24] Pierre Martre, Nadia Bertin, Christophe Salon, and Michel Génard. Modelling the size and composition of fruit, grain and seed by process-based simulation models. New Phytologist, 191(3):601–618, 2011.

[25] Julienne Fanwoua, Pieter HB de Visser, Ep Heuvelink, Xinyou Yin, Paul C Struik, and Leo FM Marcelis. A dynamic model of tomato fruit growth integrating cell division, cell growth and endoreduplication. Functional Plant Biology, 40(11):1098–1114, 2013.

[26] Michel Génard, Nadia Bertin, Charlotte Borel, Philippe Bussières, Hélène Gautier, Robert Habib, Mathieu Lechaudel, Alain Lecomte, Françoise Lescourret, Philippe Lobit, et al. Towards a virtual fruit focusing on quality: modelling features and potential uses. Journal of Experimental Botany, 58(5):917–928, 2007.

[27] Nadia Bertin, Michel Génard, and Svetlana Fishman. A model for an early stage of tomato fruit development: cell multiplication and cessation of the cell proliferative activity. Annals of Botany, 92(1):65–72, 2003.

[28] Florent Pantin, Thierry Simonneau, and Bertrand Muller. Coming of leaf age: control of growth by hydraulics and metabolics during leaf ontogeny. New Phytologist, 196(2):349–366, 2012.

[29] Huai-Feng Liu, Michel Génard, Soraya Guichard, and Nadia Bertin. Model-assisted analysis of tomato fruit growth in relation to carbon and water fluxes. Journal of experimental botany, 58(13):3567–3580, 2007.

[30] Michel Génard, Nadia Bertin, Hélène Gautier, Françoise Lescourret, and Bénédicte Quilot. Virtual profiling: a new way to analyse phenotypes. The Plant Journal, 62(2):344–355, 2010.

[31] Michel Génard, Françoise Lescourret, Nadia Bertin, and Gilles Vercambre. Resource

translocation modelling highlights density-dependence effects in fruit production at various levels of organisation. Frontiers in Plant Science, page 2391, 2022.

[32] Marion Prudent, Zhan Wu Dai, Michel Génard, Nadia Bertin, Mathilde Causse, and Philippe Vivin. Resource competition modulates the seed number–fruit size relationship in a genotype-dependent manner: A modeling approach in grape and tomato. Ecological Modelling, 290:54–64, 2014.

[33] FranÇoise Lescourret and Michel Génard. A multi-level theory of competition for resources applied to fruit production. Ecoscience, 10(3):334–341, 2003.

[34] LFM Marcelis, E Heuvelink, and J Goudriaan. Modelling biomass production and yield of horticultural crops: a review. Scientia Horticulturae, 74(1-2):83–111, 1998.

[35] PEH Minchin, MR Thorpe, and JF Farrar. A simple mechanistic model of phloem transport which explains sink priority. Journal of experimental botany, 44(5):947–955, 1993.

[36] Jean-Pierre Renaudin, Cynthia Deluche, Catherine Cheniclet, Christian Chevalier, and Nathalie Frangne. Cell layer-specific patterns of cell division and cell expansion during fruit set and fruit growth in tomato pericarp. Journal of Experimental Botany, 68(7):1613–1623, 2017.

[37] Natalia Pabón-Mora and Amy Litt. Comparative anatomical and developmental analysis of dry and fleshy fruits of solanaceae. American Journal of Botany, 98(9):1415–1436, 2011.

[38] Han Xiao, Cheryll Radovich, Nicholas Welty, Jason Hsu, Dongmei Li, Tea Meulia, and Esther Van Der Knaap. Integration of tomato reproductive developmental landmarks and expression profiles, and the effect of sun on fruit shape. BMC Plant Biology, 9:1–21, 2009.

[39] Valentina Baldazzi, Pierre Valsesia, Michel Génard, and Nadia Bertin. Organ-wide and ploidy-dependent regulation both contribute to cell-size determination: evidence from a computational model of tomato fruit. Journal of Experimental Botany, 70(21):6215–6228, 2019.

[40] Benoît Perthame. Transport equations in biology. Springer Science & Business Media, 2006.

[41] Matteo Osella, Eileen Nugent, and Marco Cosentino Lagomarsino. Concerted control of escherichia coli cell division. Proceedings of the National Academy of Sciences, 111(9):3431–3435, 2014.

[42] Zoe V Finkel, Andrew J Irwin, and Oscar Schofield. Resource limitation alters the 3/4 size scaling of metabolic rates in phytoplankton. Marine Ecology Progress Series, 273:269–279, 2004.

[43] Alessandro Concas, Massimo Pisu, and Giacomo Cao. A novel mathematical model to simulate the size-structured growth of microalgae strains dividing by multiple fission. Chemical Engineering Journal, 287:252–268, 2016.

[44] MT Allen, Przemyslaw Prusinkiewicz, and TM DeJong. Using l-systems for modeling source–sink interactions, architecture and physiology of growing trees: the l-peach model. New phytologist, 166(3):869–880, 2005.

[45] John HM Thornley and Ian R Johnson. Plant and crop modelling. Clarendon Oxford, 1990.

[46] Angharad R Jones, Leah R Band, and James AH Murray. Double or nothing? cell division and cell size control. Trends in Plant Science, 24(12):1083–1093, 2019.

[47] Johan A Metz and Odo Diekmann. The dynamics of physiologically structured populations, volume 68. Springer, 2014.

[48] Jia-Jer Liou, Friedrich Srienc, and AG Fredrickson. Solutions of population balance models based on a successive generations approach. Chemical Engineering Science, 52(9):1529–1540, 1997.

[49] Nikos V Mantzaris. Stochastic and deterministic simulations of heterogeneous cell population dynamics. Journal of theoretical biology, 241(3):690–706, 2006.

[50] Nikolaos V Mantzaris, Prodromos Daoutidis, and Friedrich Srienc. Numerical solution of multi-variable cell population balance models: I. finite difference methods. Computers & Chemical Engineering, 25(11-12):1411–1440, 2001.

[51] Angharad R. Jones, Manuel Forero-Vargas, Simon P Withers, Richard S Smith, Jan Traas, Walter Dewitte, and James AH Murray. Cell-size dependent progression of the cell cycle creates homeostasis and flexibility of plant cell size. Nature communications, 8(1):15060, 2017.

[52] Wallace F Marshall, Kevin D Young, Matthew Swaffer, Elizabeth Wood, Paul Nurse, Akatsuki Kimura, Joseph Frankel, John Wallingford, Virginia Walbot, Xian Qu, et al. What determines cell size? BMC biology, 10:1–22, 2012.

[53] Sarah Täuber, Corinna Golze, Phuong Ho, Eric von Lieres, and Alexander Grünberger. dmscc: a microfluidic platform for microbial single-cell cultivation of corynebacterium glutamicum under dynamic environmental medium conditions. Lab on a Chip, 20(23):4442–4455, 2020.

[54] Isabella Santi, Neeraj Dhar, Djenet Bousbaine, Yuichi Wakamoto, and John D McKinney. Single-cell dynamics of the chromosome replication and cell division cycles in mycobacteria. Nature communications, 4(1):2470, 2013.

[55] Gabriele Micali, Jacopo Grilli, Jacopo Marchi, Matteo Osella, and Marco Cosentino Lagomarsino. Dissecting the control mechanisms for dna replication and cell division in e. coli. Cell reports, 25(3):761–771, 2018.

[56] Giuseppe Facchetti, Fred Chang, and Martin Howard. Controlling cell size through sizer mechanisms. Current Opinion in Systems Biology, 5:86–92, 2017.

[57] Jasmien Vercruysse, Michiel Van Bel, Cristina M Osuna-Cruz, Shubhada R Kulkarni, Véronique Storme, Hilde Nelissen, Nathalie Gonzalez, Dirk Inzé, and Klaas Vandepoele. Comparative transcriptomics enables the identification of functional orthologous genes involved in early leaf growth. Plant biotechnology journal, 18(2):553–567, 2020.

[58] Peter A McAtee, Ian C Hallett, Jason W Johnston, and Robert J Schaffer. A rapid method of fruit cell isolation for cell size and shape measurements. Plant methods, 5:1–7, 2009.

[59] Leila Aslani, Thomas Breniere, Anne-Laure Fanciullino, and Nadia Bertin. Evidence of the very early effects of water deficit on cell division and expansion processes in tomato ovaries. Environmental and Experimental Botany, 207:105227, 2023.

[60] Sara C Pinto, Boris Stojilković, Xinyu Zhang, and Robert Sablowski. Plant cell size: Links to cell cycle, differentiation and ploidy. Current Opinion in Plant Biology, 78:102527, 2024.

[61] Daniel Williamson, William Tasker-Brown, James AH Murray, Angharad R Jones, and Leah R Band. Modelling how plant cell-cycle progression leads to cell size regulation. PLoS Computational Biology, 19(10):e1011503, 2023.

[62] Mochamad Apri, Johannes Kromdijk, Pieter HB de Visser, Maarten de Gee, and Jaap Molenaar. Modelling cell division and endoreduplication in tomato fruit pericarp. Journal of Theoretical Biology, 349:32–43, 2014.

[63] Maja Musse, Kévin Bidault, Stéphane Quellec, Béatrice Brunel, Guylaine Collewet, Mireille Cambert, and Nadia Bertin. Spatial and temporal evolution of quantitative magnetic resonance imaging parameters of peach and apple fruit–relationship with biophysical and metabolic traits. The Plant Journal, 105(1):62–78, 2021.

[64] LFM Marcelis and LR Baan Hofman-Eijer. Cell division and expansion in the cucumber fruit. Journal of horticultural science, 68(5):665–671, 1993.

[65] Maria C Camarero, Beatriz Briegas, Jorge Corbacho, Juana Labrador, Ángel-Carlos Román, Antía Verde, Mercedes Gallardo, and Maria C Gomez-Jimenez. Variations in fruit ploidy level and cell size between small-and large-fruited olive cultivars during fruit ontogeny. Plants, 13(7):990, 2024.

[66] Léa Roch, Sylvain Prigent, Holger Klose, Coffi-Belmys Cakpo, Bertrand Beauvoit, Catherine Deborde, Laetitia Fouillen, Pierre Van Delft, Daniel Jacob, Björn Usadel, et al. Biomass composition explains fruit relative growth rate and discriminates climacteric from non-climacteric species. Journal of experimental botany, 71(19):5823–5836, 2020.

[67] MB Tesar. Physiological basis of crop growth and development. ASA, CSSA, 1984.

[68] Mao-Song Pei, Su-Hao Cao, Lei Wu, Guo-Ming Wang, Zhi-Hua Xie, Chao Gu, and Shao-Ling Zhang. Comparative transcriptome analyses of fruit development among pears, peaches, and strawberries provide new insights into single sigmoid patterns. BMC plant biology, 20:1–15, 2020.

[69] Ken N Paige. Overcompensation, environmental stress, and the role of endoreduplication. American journal of botany, 105(7):1105–1108, 2018.

[70] Christian Chevalier, Mehdi Nafati, Elodie Mathieu-Rivet, Matthieu Bourdon, Nathalie Frangne, Catherine Cheniclet, Jean-Pierre Renaudin, Frédéric Gévaudant, and Michel

Hernould. Elucidating the functional role of endoreduplication in tomato fruit development. Annals of Botany, 107(7):1159–1169, 2011.

[71] Xue An, Zhiguo Li, Gabi Wegner, and Manuela Zude-Sasse. Effect of cell size distribution on mechanical properties of strawberry fruit tissue. Food Research International, 169:112787, 2023.

[72] Artur Zdunek and Mikio Umeda. Influence of cell size and cell wall volume fraction on failure properties of potato and carrot tissue. Journal of Texture Studies, 36(1):25–43, 2005.

[73] P Allan-Wojtas, KA Sanford, KB McRae, and S Carbyn. An integrated microstructural and sensory approach to describe apple texture. 2003.

[74] Cheng Chen, Joshua S MacCready, Daniel C Ducat, and Katherine W Osteryoung. The molecular machinery of chloroplast division. Plant physiology, 176(1):138–151, 2018.

[75] Kumiko Okazaki, Yukihiro Kabeya, Kenji Suzuki, Toshiyuki Mori, Takanari Ichikawa, Minami Matsui, Hiromitsu Nakanishi, and Shin-ya Miyagishima. The plastid division1 and 2 components of the chloroplast division machinery determine the rate of chloroplast division in land plant cell differentiation. The Plant Cell, 21(6):1769–1780, 2009.

[76] Michael A Henson. Dynamic modeling of microbial cell populations. Current opinion in biotechnology, 14(5):460–467, 2003.

[77] Nikolaos V Mantzaris, Jia-Jer Liou, Prodromos Daoutidis, and Friedrich Srienc. Numerical solution of a mass structured cell population balance model in an environment of changing substrate concentration. Journal of Biotechnology, 71(1-3):157–174, 1999.

[78] Jérôme Morchain, Maxime Pigou, and Noureddine Lebaz. A population balance model

for bioreactors combining interdivision time distributions and micromixing concepts. Biochemical engineering journal, 126:135–145, 2017.

[79] Fabio R Sidoli, A Mantalaris, and SP3449502 Asprey. Modelling of mammalian cells and cell culture processes. Cytotechnology, 44(1):27–46, 2004.

[80] Pablo Bravo, Siu Lung Ng, Kathryn A MacGillivray, Brian K Hammer, and Peter J Yunker. Vertical growth dynamics of biofilms. Proceedings of the National Academy of Sciences, 120(11):e2214211120, 2023.

[81] Chiara Enrico Bena, Marco Del Giudice, Alice Grob, Thomas Gueudré, Mattia Miotto, Dimitra Gialama, Matteo Osella, Emilia Turco, Francesca Ceroni, Andrea De Martino, et al. Initial cell density encodes proliferative potential in cancer cell populations. Scientific Reports, 11(1):6101, 2021.

[82] RI Grange and J Andrews. Respiration and growth of tomato fruit. Plant, Cell & Environment, 18(8):925–930, 1995.

[83] Irina Pavelescu, Josep Vilarrasa-Blasi, Ainoa Planas-Riverola, Mary-Paz González-García, Ana I Caño-Delgado, and Marta Ibañes. A sizer model for cell differentiation in arabidopsis thaliana root growth. Molecular systems biology, 14(1):e7687, 2018.

[84] L M Berliner. Physical-statistical modeling in geophysics. J Geophys Res, 108:8776, 2003.

[85] S Soubeyrand, A-L Laine, I Hanski, and A Penttinen. Spatiotemporal structure of host-pathogen interactions in a metapopulation. American Naturalist, 174(3):308–320, Sep 2009.

[86] J.M. Marin and C. P. Robert. Bayesian Core. Springer, New York, NY, 2007.